A Statistical Radio Range Model for a Robot MANET in a Subterranean Mine

Manoja D. Weiss, *Member, IEEE*, James Peak, and
Thomas Schwengler, *Senior Member, IEEE*

***Abstract*—We present a statistical model for the radio range between robots in a Mobile Ad hoc NETwork (MANET) deployed in an underground mine. Such unmanned mobile robotic networks could potentially be used in hazard mitigation and search and rescue in tunnel environments such as mines and subways, as well as in building environments. In addition to fading characteristics, our model is able to represent the variable nature of the propagation path-loss exponent. To support our model, we present path-loss measurements made in a real mine. The usefulness of our model lies in the fact that it represents an overall propagation model for a mine and therefore can be used to calculate the wireless connectivity probability of an arbitrary node in the network without requiring a detailed physical representation of the MANET within the mine.**

***Index Terms*—Mine tunnels, path-loss exponent, path-loss model, radio propagation, wireless connectivity.**

I. Introduction

THE ABILITY to model a robot Mobile Ad hoc NETwork (MANET) in a realistic propagation environment is necessary to determine its wireless connectivity probability in that environment. As stated in [1], the wireless connectivity probability, or simply connectivity, of a node in a wireless sensor network represents a measure of the percentage of time that the node is connected to at least one other node. It can also be described as the likelihood of the nodes being in each other's radio range. A high connectivity probability is required for most real-time communications, such as streaming video. To increase node connectivity, a higher density of nodes, higher transmit power, higher gain antennas, or more sensitive receivers could be used since each of these factors increases the likelihood that nodes are within radio range of each other. It is therefore of interest to find the connectivity probability as a function of these parameters. To achieve this goal, a reasonable model of the radio range in the particular environment is necessary.

General methods of improving the connectivity of mobile robot networks have been previously published, as in [2] and [3], but with no consideration of realistic propagation models. In [1], the wireless connectivity of a robot MANET is calculated based on a radio range model that includes Rayleigh fading. This radio range model is well suited for most open-area environments with a free-space path-loss exponent of $n = 2$ containing scatterers that give rise to Rayleigh fading. However, considering a MANET of robots exploring a subterranean environment such as a mine, each robot pair will experience unique propagation characteristics that are quite different from free space. In particular, there will be waveguiding along straight tunnels that give a reduced path loss compared to free space and nonline-of-sight (NLOS) propagation in nonlinear tunnel geometries, such as bends and branches, that result in a higher path loss compared to free space. Rayleigh fading alone will not accurately represent this propagation channel. We present a model that includes both Rayleigh fading and *a random path-loss exponent* to represent the variable path-loss characteristics across the mine. This allows us to create a stochastic propagation model for the mine as a whole. This approach is similar to a previous method known as "physical–statistical modeling," which is used in modeling citywide satellite communications, as published in [4]–[6]. In this previous work, the communications link is dominated by diffraction from rooftops; therefore, a distribution of building heights is used to represent the variability in propagation characteristics across the city. We do not, at this time, attempt to represent the variability of the mine environment using a distribution of geometrical features such as the radius of curvature of tunnel bends/branches; instead, we use a path-loss-exponent distribution.

Models of radio propagation in underground mines have been investigated by several researchers from several countries. Theoretical work on guided-wave propagation in straight mine tunnels leading to a path loss that is less than the free-space loss is discussed in detail in [7]–[11]. The extra losses due to diffraction at junctions and corners are discussed in [7] and [12]–[16]; curved tunnels are discussed in [11] and [17]–[20]. Measured statistical results for fast-fading distributions in various sections of mine tunnels are found in [9], [12], [21], and [22]. However, to the best of our knowledge, there is currently no model that attempts to represent the mine as a whole since the conditions are varied depending on the local layout of different areas of the mine. In this paper, we propose one way in which a statistical model can be built to represent the entire mine environment and thereby build a realistic simulation environment for subterranean tunnel robot MANETs. The work presented here is also applicable to other tunnel-like environments, such as building hallways and subway systems.

Manuscript received December 19, 2006; revised July 13, 2007 and September 25, 2007. This work was supported in part by the Colorado School of Mines and by the Colorado Institute of Technology under Grant 4230427. The review of this paper was coordinated by Prof. Z. Yun.

M. D. Weiss is with the Colorado School of Mines, Golden, CO 80401 USA (e-mail: mweiss@mines.edu).

J. Peak is with Lockhead Martin Space Systems Company Communications, Denver, CO 80201 USA.

T. Schwengler is with Qwest Communications, Denver, CO 80202 USA.

Color versions of one or more of the figures in this paper are available online at http://ieeexplore.ieee.org.

Digital Object Identifier 10.1109/TVT.2007.912606

II. Basic Radio Range Model for a Given Path Between Two Points in a Mine

Based on measurements, we assume that, *for a given path between two points* in a mine environment, the radio range can be obtained from a statistical propagation path-loss model of the form

$$P_r = \frac{\kappa^2 \alpha^2}{d^n} P_t \tag{1}$$

where P_r is the received power, P_t is the transmitted power, α^2 is a constant that contains antenna gain and wavelength information, d is the distance between the transmitter and receiver, n is a constant path-loss exponent, and κ is a randomly distributed amplitude gain representing fading characteristics.

The amplitude gain of the path κ is assumed to be Rayleigh distributed with probability density function (pdf) defined as

$$f_K(\kappa) = \frac{\kappa}{\sigma^2} e^{(-\kappa^2/2\sigma^2)} \tag{2}$$

where

$$\sigma^2 = \frac{\langle \kappa^2 \rangle}{2} \tag{3}$$

and $\langle\ \rangle$ denotes the expected value or statistical average. We follow the procedure in [1] and define a "lossless path" as one in which $\langle \kappa^2 \rangle = 1$, corresponding to $\sigma = 0.7071$. Note that, for this case, $\langle \kappa \rangle = \sigma\sqrt{\pi/2} = 0.8862$. All calculations in this paper set $\sigma = \sqrt{0.5} = 0.7071$.

Let us now define parameter R_0 as the idealized free-space radio range, which is the maximum distance at which radio communications is possible in free space $(n = 2)$ *in the absence of fading*. It is obtained from the Friis formula by solving for d when the received power is the minimum that is detectable by the receiver. For a specific wavelength, a given set of antennas, a specific transmitter power, and the minimum detectable power level $P_{r,\min}$, R_0 is defined by

$$R_0^2 = \frac{P_t}{P_{r,\min}} \alpha^2. \tag{4}$$

R_0 is a measure of the transmit power, antenna gain, and receiver sensitivity $(1/P_{r,\min})$ of the nodes and is dependent on frequency through variable α. In the calculations and simulations that follow, we find, for a given frequency, the radio range in the presence of Rayleigh fading and any n and express it in terms of R_0. We also investigate the effect of varying R_0 on the connectivity probability. This is equivalent to investigating the effects of varying the transmit power, antenna gain, receiver sensitivity, or all three. If the frequency is varied, in addition to changing R_0, n and κ may need to be changed as well since the propagation properties may be different.

Radio range R is the maximum distance at which radio communications is possible in the presence of Rayleigh fading and for any general path-loss exponent n. For the statistical model given in (1), the radio range can be written as a function of random variable κ as follows:

$$R(\kappa) = (\kappa R_0)^{2/n}. \tag{5}$$

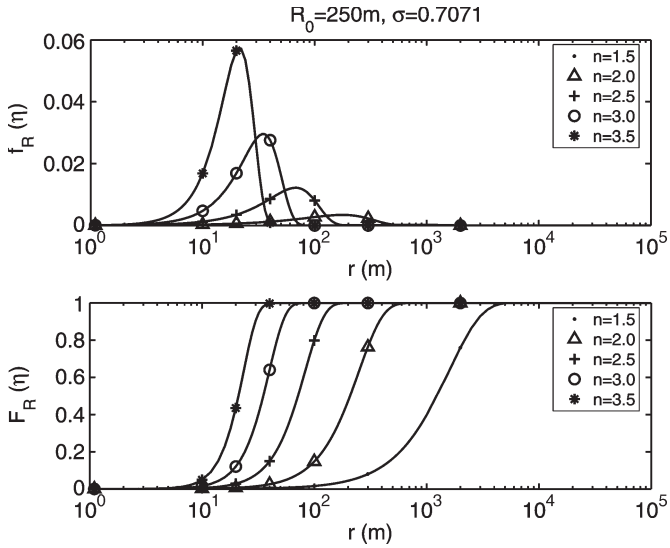

Fig. 1. Weibull (top) pdfs and (bottom) cdfs for $R_0 = 250$ m and several values of n.

If we define another parameter r_0 as

$$r_0 = R_0^{2/n} \tag{6}$$

the maximum radio range can be expressed as

$$R(\kappa) = \kappa^{2/n} r_0. \tag{7}$$

This is a function of a random variable κ and therefore has a pdf given by

$$f_R(r) = f_K(\kappa) \frac{d\kappa}{dR} \tag{8}$$

where r are the specific values that R can take. Upon simplification, we obtain a Weibull pdf for R, i.e.,

$$f_R(r) = \frac{n r^{n-1}}{2 r_0^2 \sigma^2} e^{(-r^n/2r_0^2\sigma^2)}. \tag{9}$$

The Weibull pdfs and cumulative distribution functions (cdfs) for various values of n are calculated and shown in Fig. 1. The peak of the Weibull pdf, representing the mode of the data or the most common value of radio range, shifts to lower values of r as the path-loss exponent increases from $n = 1.5$ to $n = 3.5$. This leftward shift is mirrored in the cdf: The median value, which is given by cdf $= 50\%$, is reduced from over 1 km to about 20 m.

The mean or expected value of the radio range $\langle R \rangle$ is obtained from the Weibull pdf in terms of the fading statistics and parameter R_0 as

$$\langle R \rangle = \langle k^{2/n} \rangle {R_0}^{2/n}. \tag{10}$$

The expected range as a function of path-loss exponent is plotted in Fig. 2. For free space, $\langle R \rangle = \langle k \rangle R_0 = 0.8862\ R_0$. This shows that Rayleigh fading causes the range in free space to be reduced to about 89% of the value it would have without fading. For $n < 2$, the expected range is larger than R_0, because the received power increases more gradually with distance. When $n = 3.5$, the received power rapidly decreases, and the

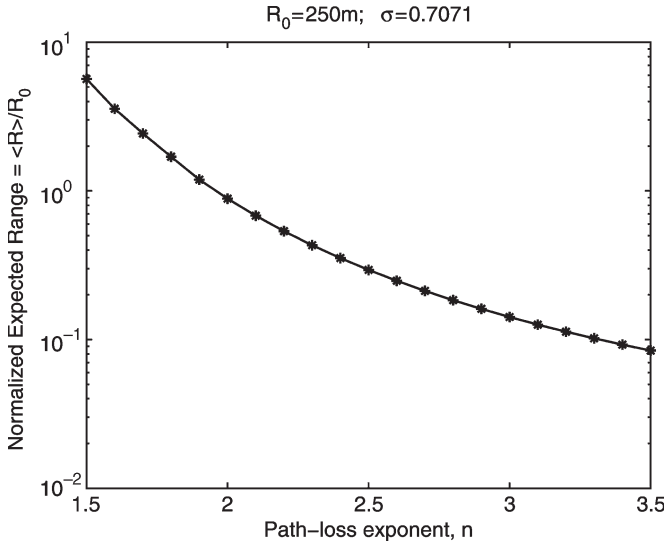

Fig. 2. Relationship between the expected range and the path-loss exponent. The expected range is normalized to R_0, which is the idealized free-space range in the absence of fading.

expected range is less than 10% of R_0. The mode, mean, and median ranges are approximately the same for this distribution.

We point out that this radio range model may become inaccurate at extremely long ranges (typically > 1 km). Close to the transmitter, a plethora of higher order modes is typically excited by the antenna, and the attenuation can be represented by the model given here. Far from the transmitter, the propagation mechanism changes, due to the higher order modes giving way to one or two low-loss modes where attenuation exponentially varies with distance, instead of according to the power law in (1). This near-zone/far-zone propagation and the breakpoint between zones are more thoroughly described in [10] and [11]. For the mine environment that we describe, the average tunnel lengths are not more than about 50–100 m; therefore, we can assume that the receiver will most likely be in the near-zone of the transmitter where the power law holds.

III. Measurements of Path Loss at the Edgar Experimental Mine

Measurements were conducted at the Colorado School of Mines' Edgar Experimental Mine to determine the variable nature of the fading statistics and the path-loss exponent n. For a fixed transmitter and a mobile receiver, received power measurements were recorded in three different tunnels: 1) a straight tunnel; 2) a slightly bent tunnel; and 3) a path extending from the main tunnel into a branch tunnel. Fig. 3 shows these tunnels on a map of the Edgar Mine. These three tunnels were chosen to sample an extremely low path loss (along the straight tunnel) and an extremely high path loss (along the branched path). We assume that these represent two extreme cases of path loss that could be encountered between two nodes in a MANET and therefore serve to define the minimum and maximum values of n in this particular environment. The slightly bent tunnel was chosen to determine the effect of NLOS propagation in tunnels whose geometry is only slightly perturbed in comparison with a straight line.

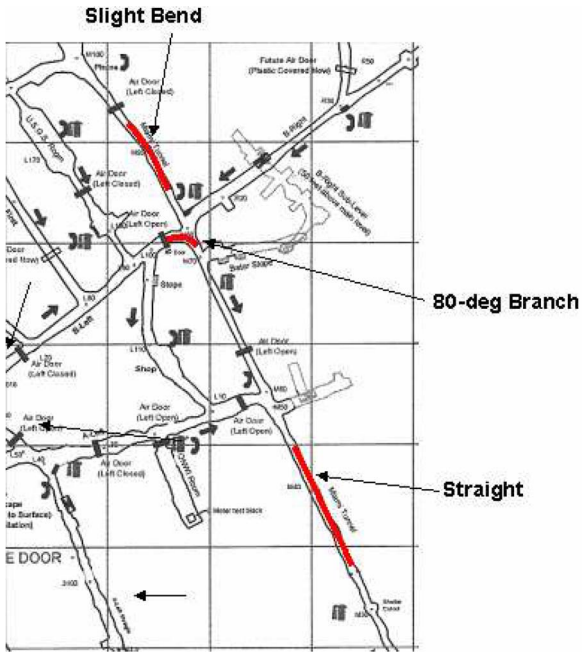

Fig. 3. Map of the Miami Tunnel in the Edgar Experimental Mine belonging to the Colorado School of Mines. The measurement locations are shown in thick lines. The tunnels are about 3 m in width and height, on average, with rounded corners and walls, which are quite rough and irregular in the cross section.

An HP8673M signal generator was used to excite a horizontally polarized Ant-Corp 1–12-GHz log-periodic antenna at a height of approximately 0.75 m from the ground. The tunnel varies in cross-sectional area throughout the measurement space, but it is, on average, 3 m wide by 3 m high. The received power was measured by an HP8484A 0.01–18-GHz thermocouple power sensor connected to an HP437B power meter with a horizontally polarized Ant-Corp 1–12-GHz log-periodic antenna at the same height as the transmitter. The transmitter was stationary, whereas the receiver was moved along a horizontal path at the approximate lateral center of the tunnel. The path length was increased until the sensitivity of the power sensor (-75 dBm) was reached or the path ended. Measurements were taken at 2.4 and 5 GHz.

The data gathered from the measurements previously described were fitted to the expression

$$P_{\text{fit}} = \frac{\alpha^2}{R^n} P_t \tag{11}$$

to find the unknowns α and n. The fit was constrained such that α was the same for each data set, so that the fading statistics would remain the same for each path. However, the value of n is unique to each path. The data and the corresponding fitted curves are shown in the log–log plots of Figs. 4 and 5. n is given by the negative slope of the log–log plots, whereas α^2 is given by the intercept. The horizontal axis represents the curvilinear distance along the path between the transmitter and receiver and not the Euclidean distance. As this figure shows, the data can be fitted to the basic path-loss model with constant n, which was described in the previous section. It is interesting to see, although perfectly reasonable, that the path-loss exponent increases with the severity of the bend or, in other words, the

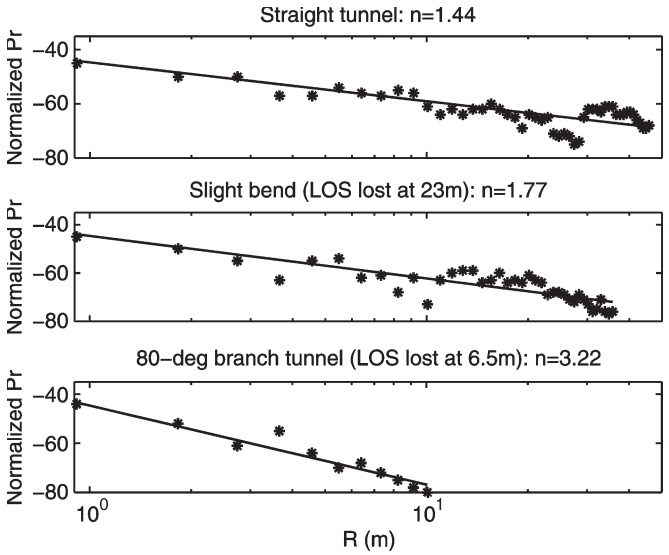

Fig. 4. Received power measurements at 2.4 GHz in the Miami Tunnel of the Edgar Experimental Mine. The horizontal axis represents the curvilinear distance along the path between the transmitter and receiver.

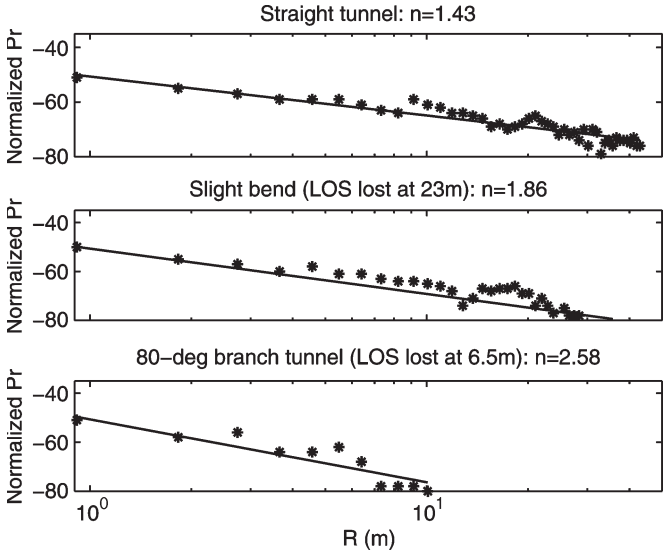

Fig.5. Received power measurements at 5 GHz in the Miami Tunnel of the Edgar Experimental Mine. The horizontal axis represents the curvilinear distance along the path between the transmitter and receiver.

inverse of the radius of curvature of the tunnel. The straight tunnel exhibits $n < 2$, which is consistent with guided-wave propagation effects in tunnels, as demonstrated in [10] and, in particular, [12], where it is noted that n is a function of polarization as well: Typically, horizontal polarization gives lower values than vertical polarization. The additional diffraction loss in the bent tunnel leads to an increased $n > 2$, as measured in [12] and [23]. The slight bend does not appear to significantly increase n.

The slope of the bend at 5 GHz is less than the slope at 2.4 GHz. Decreasing attenuation with increasing frequency in straight tunnels has been shown to be possible in [8]. However, it is curious that, in our measurements, this effect is significant for the bent tunnel but is seen only extremely slightly in the straight tunnel and not at all in the second tunnel. We hope to perform more 5-GHz measurements to investigate this further.

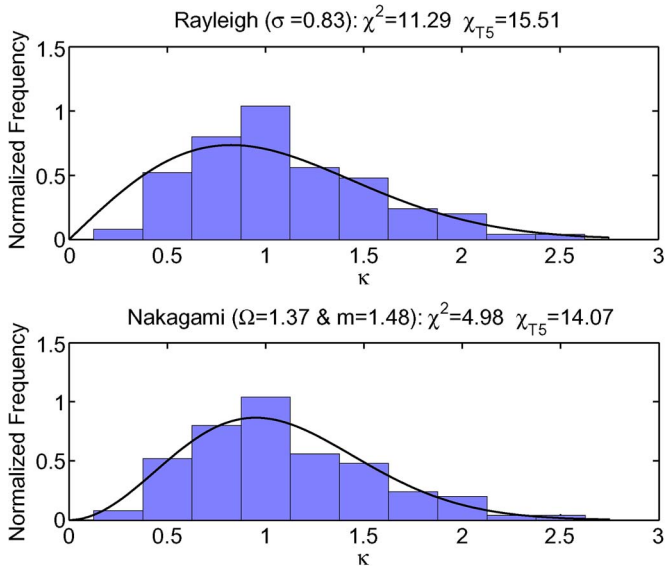

Fig. 6. Measured 2.4-GHz fading distribution at the Edgar Mine. Rayleigh and Nakagami distributions satisfy a 5% χ^2 threshold.

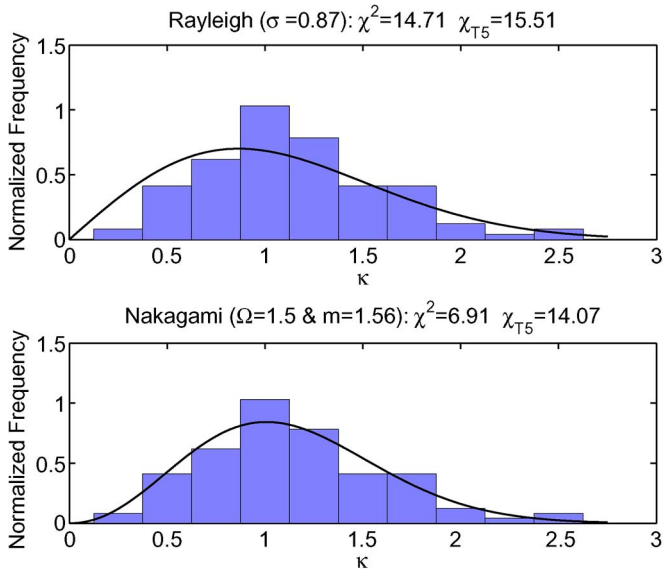

Fig. 7. Measured 5-GHz fading distribution at the Edgar Mine. Rayleigh and Nakagami distributions satisfy a 5% χ^2 threshold.

The values of n obtained at 2.4 GHz in the mine were supported by similar measurements in straight and bent portions of the basement hallway of the Engineering building at the Colorado School of Mines.

The data were also used to test two different fading distributions. First, we recognize that κ is given by the square root of the ratio of the measured data given by (1) to the fitted data given by (11). This is mathematically expressed as

$$\sqrt{\left(\frac{P_r}{P_{\text{fit}}}\right)} = \sqrt{(\kappa^2)} = \kappa. \tag{12}$$

Figs. 6 and 7 show histograms of κ for the *combined data* from all three paths at each frequency. A χ^2 goodness-of-fit calculation was performed for both a Rayleigh distribution and a more general Nakagami distribution [24], which can

be used to represent Rayleigh or Rician characteristics. The Nakagami distribution and the relevant parameters are given by the following set of expressions. When $m > 1$, the distribution is Rician, whereas $m = 1$ represents a Rayleigh distribution. Note that $\Omega = 2\sigma^2$. Thus

$$\Omega = \langle \kappa^2 \rangle$$
$$m = \frac{\Omega^2}{\langle \kappa^2 - \Omega^2 \rangle}$$
$$f_K(\kappa) = \frac{2m^m \kappa^{2m-1}}{\Gamma(m)\Omega^m} e^{-m\kappa^2/\Omega}. \tag{13}$$

The mean-square value of the measured κ data set is used to find Rayleigh parameter σ and Nakagami parameters Ω and m. These values are shown with the plots in Figs. 6 and 7. As can be seen, the χ^2 value for both the Rayleigh and Nakagami distributions is less than the 5% significance χ_t threshold, indicating that either could be used to model the fast fading. The σ value for the Rayleigh distribution is slightly greater than the "lossless" value of 0.7071, indicating that a Rician distribution is more applicable. This is corroborated in the Nakagami distribution, which has $m > 1$, indicating a Rician distribution. Although a Rician distribution may be slightly more suitable, given this set of data, it must be noted that the data include only one tunnel representing NLOS propagation. Therefore, it is reasonable to suppose that line-of-sight (LOS) behavior dominates the statistics, leading to a Rician distribution. If more tunnels with bends were included in the data, the distribution may tend toward being more Rayleigh-like. The Rayleigh distribution has been shown to be a better fit for NLOS tunnels, whereas a Rician distribution has been shown to be a better fit for LOS tunnels [22]. When LOS and NLOS tunnels are considered together as a composite environment, the density of bends within the tunnel system may dictate the tendency toward either Rayleigh or Rician behavior. This could be determined in the future through a thorough measurement campaign. In this paper, for simplicity and comparison with [1], we have assumed a Rayleigh distribution in the following analysis to demonstrate the process of obtaining the final statistical radio range model. The method could be applied to other fading distributions as well.

IV. Proposed Radio Range Model for the Mine Environment

In the previous section, we discussed how the path-loss exponent for a given path between two points could be represented by a constant value n. To model a mobile wireless network that spans the entire mine environment, we must be able to represent the variability inherent in having many possible paths of different values of n. We will therefore assume that the path-loss exponent for the entire mine can be represented by a random variable N. For simplicity, we will assume a uniform distribution for N with mean μ and width W. This pdf can be expressed as

$$f_N(n) = \begin{cases} \frac{1}{W}, & \text{if } \mu - \frac{W}{2} \le n \le \mu + \frac{W}{2} \\ 0, & \text{otherwise.} \end{cases} \tag{14}$$

Radio range R now becomes a function of two random variables: κ and N. By solving for R in (1) and using the definition of R_0, we obtain the following equation for R:

$$R(\kappa, N) = (\kappa R_0)^{2/N}. \tag{15}$$

To find the pdf of R, which is now a function of two random variables, we use the Jacobian technique [25]. This involves mapping the domain of the two independent random variables κ and N to two functions R (our radio range) and S (a dummy function), with a one-to-one mapping. Then, by finding the joint pdf $f_{R,S}(r, s)$, we obtain the marginal pdf $f_R(r)$.

First, dummy function S is defined as

$$S(\kappa) = \kappa R_0 \tag{16}$$

to simplify the computation of the joint pdf. We recognize that the joint pdf is given by

$$f_{R,S}(r, s) = \frac{f_{K,N}(\kappa, n)}{\|J\|} \tag{17}$$
$$= \frac{f_K(\kappa) f_N(n)}{\|J\|}. \tag{18}$$

The determinant of the Jacobian J is given by

$$\|J\| = \det \begin{bmatrix} \frac{\partial R}{\partial \kappa} & \frac{\partial R}{\partial N} \\ \frac{\partial S}{\partial \kappa} & \frac{\partial S}{\partial N} \end{bmatrix} \tag{19}$$
$$= \frac{R_0 R \left(\ln(R)\right)^2}{2\left(\ln(S)\right)}. \tag{20}$$

Therefore, the joint pdf becomes

$$f_{R,S}(r, s) = \frac{2\left(\ln(s)\right)}{R_0 r \left(\ln(r)\right)^2} f_K(\kappa) f_N(n). \tag{21}$$

Using (15) and (16) to transform (21) into the R, S domain, we obtain

$$\kappa = \frac{S}{R_0} \tag{22}$$
$$N = \frac{2\left(\ln(S)\right)}{\ln(R)}. \tag{23}$$

The Rayleigh pdf of κ in (2) now becomes

$$f_K\left(\frac{s}{R_0}\right) = \frac{s}{R_0 \sigma^2} e^{\frac{-s^2}{2R_0^2\sigma^2}} \tag{24}$$

and the uniform pdf for n in (14) becomes

$$f_N\left(\frac{2\ln(s)}{\ln(r)}\right) = \begin{cases} 0, & \text{if } \frac{2\ln(s)}{\ln(r)} < n_{\min} \\ 0, & \text{if } \frac{2\ln(s)}{\ln(r)} > n_{\max} \\ \frac{1}{W}, & \text{otherwise} \end{cases}$$
$$= \begin{cases} 0, & \text{if } s < r^{n_{\min}/2} \\ 0, & \text{if } s > r^{n_{\max}/2} \\ \frac{1}{W}, & \text{otherwise.} \end{cases} \tag{25}$$

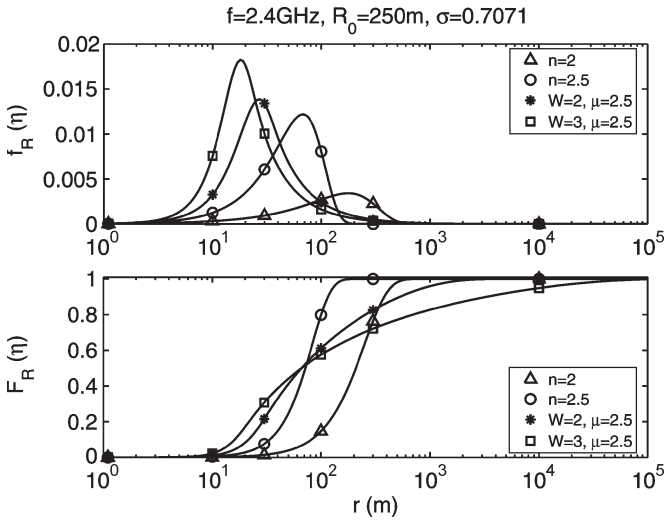

Fig. 8. (Top) PDFs and (bottom) cdfs for several propagation environments at 2.4 GHz, with a 250-m idealized fading-free free-space range.

In the preceding equation, $n_{\max} = \mu + W/2$ and $n_{\min} = \mu - W/2$ represent the upper and lower limits of the uniform N-distribution, respectively.

The joint pdf of (21) can now be purely expressed in terms of R and S according to (24) and (25). Subsequently, the desired marginal pdf is obtained from the definition

$$f_R(r) = \int_{-\infty}^{\infty} f_{R,S}(r,s)ds.$$

This expression, when integrated, results in the following final expression for the pdf of the radio range in a subterranean mine:

$$f_R(r) = \frac{\Delta}{r\left(\ln(r)\right)^2} \int_{r^{n_{\min}/2}}^{r^{n_{\max}/2}} s\left(\ln(s)\right) e^{\frac{-s^2}{2R_0^2\sigma^2}} ds. \qquad (26)$$

In the preceding equation, $\Delta = (2/WR_0^2\sigma^2)$. The expression must be numerically integrated for each value of r.

The expression in (26) is verified by using it to represent constant path-loss exponents and comparing with the Weibull distribution derived in (9). A constant path-loss exponent is represented as a very narrowly distributed uniform distribution around the desired path exponent. For example, the pdf for $n = 2$ is numerically obtained by using $(W = 0.001, \mu = 2)$ in (26) and is found to be identical to that obtained from the Weibull distribution in (9). We verified this for a wide range of values of n.

Fig. 8 explores the effect of varying W and μ on the pdfs and cdfs of radio range by comparing four propagation models, using (26). These models include the following: 1) free space or $n = 2$ $(W = 0.001, \mu = 2)$; 2) $n = 2.5$ $(W = 0.001, \mu = 2.5)$; 3) $(W = 2, \mu = 2.5)$; and 4) $(W = 3, \mu = 2.5)$. In this figure, the mode, which is the most common value of radio range, shifts to lower values as μ and W increase. It is interesting to note that the median value given by cdf $= 50\%$ is approximately the same for all three cases where $\mu = 2.5$, even though the shape of the cdfs and expected range, or mean, for these cases are quite different. The expected ranges for the four models are 222, 74, 201, and 1931 m, respectively. Model 1 has a higher median value of range than the other models. Model 2 shows a highly reduced expected range compared to models 3 and 4 since the lower values of n encountered in the mine are not considered. Models 3 and 4, on the other hand, have increased expected range compared to models 1 and 2 due to the inclusion of lower n values. However, model 4 is not realistic since it includes values of path-loss exponent of as low as $N = 1$, which is lower than the measured values and would therefore skew the results in favor of unrealistically longer ranges, as shown by its cdf in Fig. 8. We propose model 3 as the most appropriate for the 2.4-GHz Edgar Mine environment since it is approximately bounded by the lowest (1.44) and highest (3.22) measured values of path-loss exponent.

We emphasize that the uniform distribution for N is merely a starting point. It is used to illustrate the technique and effects of incorporating a random value of N into the radio range model. A Gaussian distribution may be more suitable, as indicated by measurements conducted in suburban areas [26]. The distribution will primarily depend on parameters such as the frequency, average length of straight tunnels, and the geometrical attributes and density of bends and curves encountered in the mine. For example, if the straight tunnel segments in a mine are very short, the distribution of N may favor larger values since there will typically be a bend in the path between two radio nodes. If the straight tunnel segments are very long on average, then the N-distribution may favor lower values. A thorough measurement campaign is necessary to define and refine the most realistic shape of the N-distribution within a mine.

Additionally, more measurements are required to better understand the propagation trends at 5 GHz. The general trends of the slopes for straight and bent tunnels at 2.4 GHz were verified with hallway measurements as well, whereas the 5-GHz measurements were limited to the three mine tunnels described in this paper. Therefore, for the rest of this discussion, we will limit ourselves to 2.4-GHz propagation.

V. Application of the Proposed Radio Range Model to a Robot MANET

We use the proposed radio range model of (26) to find the connectivity probability of a 1-D robot MANET in a subterranean mine: a single chain of robots along a physical path that could be along two or three dimensions, as shown in Fig. 9.

Our simulations follow the steady-state connectivity analysis described in [1]. We will briefly outline the general procedure, but a more detailed description can be found in [1]. For a MANET that is changing with time, at each time step, each node either remains stationary or moves forward or backward along the 1-D path. As time goes to infinity, the probabilities of moving forward, backward, or not moving approach *stationary steady-state probabilities* that describe the percentage of time in which the node is moving forward, moving backward, or choosing to stay in the same position. These stationary steady-state probabilities form the basis for a probabilistic mobility model. By combining this mobility model with an appropriate radio range model and assuming that all nodes are statistically

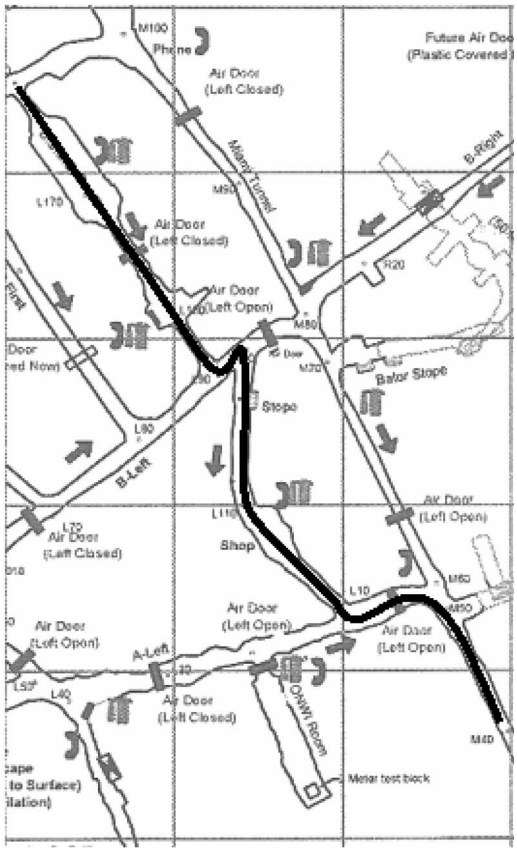

Fig. 9. Example of a possible physical layout for a 1-D robot MANET. The physical 2-D space is "unwrapped" into the 1-D simulation space along the path.

independent, the connectivity probability of a single node a in the MANET is obtained in [1] as

$$\begin{aligned} C_a &= 1 - \overline{C}_a \\ &= 1 - \prod_{b=1, b\neq a}^{Z} (1 - c_{ab}) \\ &= 1 - (1 - c_{ab})^{Z-1} \end{aligned} \tag{27}$$

where Z is the total number of mobile agents in the network. C_a is the probability that node a is connected to at least one other node in the network, whereas $\overline{C}_a$ represents the probability that it is not. c_{ab} is the one-hop connectivity of node a with respect to node b and is given by the probability that the physical separation R_{ab} is less than or equal to the transmission range.

It is shown in [1] that

$$\begin{aligned} c_{ab} &= P(R_{ab} \leq r) \\ &= \int_0^{\infty} P\left(R_{ab} \leq r | r\right) f_R(r) dr \\ &= \sum_{x_b=0}^{M} \left[\sum_{x_a=0}^{M} \left(\int_{R_{ab}}^{\infty} f_R(r) dr \right) \pi_{x_a} \right] \pi_{x_b}. \end{aligned} \tag{28}$$

M is the maximum distance along the path. The positions of nodes a and b along the path are given as x_a and x_b, respectively, such that $0 \leq x_a, x_b \leq M$. The increment used for x_a and x_b is unity, although a smaller value could be used for increased resolution. π_{x_a} and π_{x_b} are the position-dependent parameters of the mobility model. $f_R(r)$ is the pdf of the radio range. Since c_{ab} is the probability that the nodes are within radio range, the integral is evaluated from R_{ab} to ∞ since, for $r < R_{ab}$, there is zero probability of being connected.

For our simulations, $f_R(r)$ is given by (26), and connectivity probability C_a is calculated for a physical space $M = 1000$ m, using the four different uniform distributions of N described in the previous section. Results are shown in Figs. 10 and 11.

The simulation results in Fig. 10 reveal a strong correspondence between R_0 and network connectivity C_a. Recall that R_0 is a parameter that represents transmit power, antenna gain, and receiver sensitivity for a given frequency. The increase in connectivity as R_0 increases is evident for all propagation models. This means that connectivity can be increased by increasing

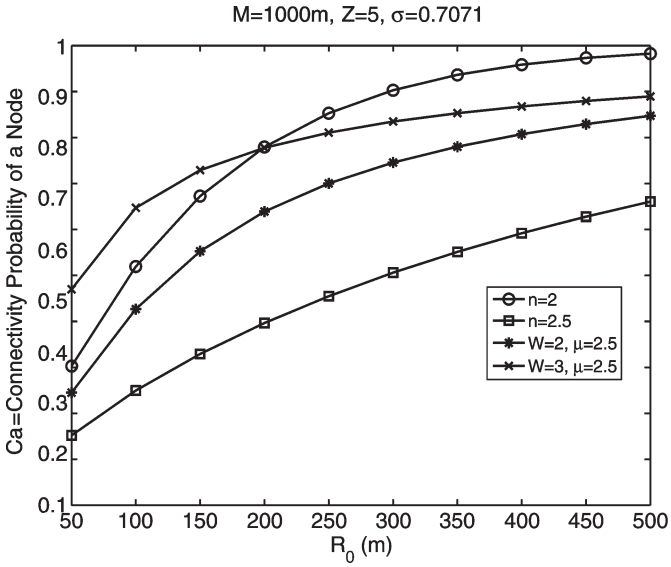

Fig. 10. Connectivity as a function of the idealized fading-free free-space transmission range R_0.

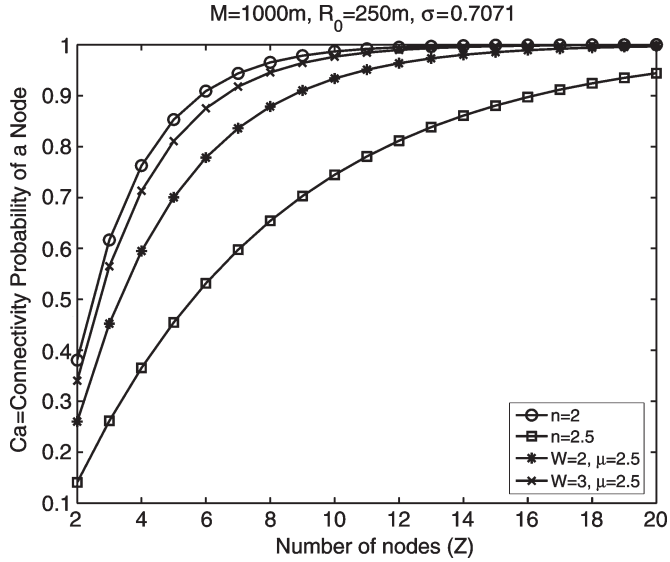

Fig. 11. Connectivity as a function of the number of robots.

transmit power, antenna gain, receiver sensitivity, or some combination of these. When $n = 2.5$, the connectivity is about 65%, whereas the free-space case gives more than 95%. The $(W = 2, \mu = 2.5)$ case shows connectivity values between the free-space and $n = 2.5$ cases for all values of R_0. However, the $(W = 3, \mu = 2.5)$ case gives a connectivity curve that is higher than the free-space curve for low R_0 and between the free-space and $(W = 2, \mu = 2.5)$ case for high R_0. The reason for this is that the $W = 3$ case includes extremely low values of path-loss exponent that correspond to very large values of range and, therefore, to high connectivity probability. However, as stated in the previous section, this model is not an accurate representation of the mine since it includes values of N that are lower than the lowest measured value of approximately $N = 1.5$. The $(W = 2, \mu = 2.5)$ model is more reasonable for application in the mine, because it spans values of N that are approximately within the measured limits.

The effect of varying the number of robots is shown in Fig. 11. As expected, a larger number of robots within the space M is equivalent to having a larger node density and therefore increases the connectivity probability. To obtain a MANET with connectivity that is greater than 95%, a free-space environment would require at least seven robots, an environment with $n = 2.5$ would require more than 20 robots, an environment with $(W = 2, \mu = 2.5)$ would require at least 11 robots, and an environment with $(W = 3, \mu = 2.5)$ would require at least eight robots. These numbers will change if R_0 is changed by varying the frequency, transmit power, antenna gain, or receiver sensitivity.

The aforementioned simulations show that the effects of an N-distribution are unique in comparison with a constant path-loss exponent, even if the mean of the distribution $(\mu = 2.5)$ is the same as the constant value $n = 2.5$. As shown in Figs. 10 and 11, the connectivity for the $n = 2.5$ case is quite different in behavior and value compared to both $\mu = 2.5$ cases. This suggests that the mean value of the experimental path-loss exponents does not adequately represent the entire mine environment.

As shown in the preceding plots, the specific distribution assumed for N—whether a constant or a uniform distribution of given specifications—plays a big role in determining the value of the connectivity probability at a particular R_0. Therefore, it is important to develop reasonable distributions for both N and fast fading, based on extensive measurements of characteristic mines.

VI. Conclusion

In this paper, we propose the use of a new radio range model to represent a subterranean mine, which is a widely variable propagation environment. The novelty of this radio range model is its consideration of a random distribution of path-loss exponents to represent the variable nature of propagation loss along different paths in the mine. Using our model, we simulate a 1-D robot MANET and show that the connectivity probability is quite dependent on the properties of the path-loss exponent distribution. The radio range model discussed in this paper is also applicable to subways and hall environments where the navigation pathways are tunnel-like.

Acknowledgment

The authors would like to thank D. Mosch for the access to the Edgar Mine, Prof. J. Steele and Prof. K. Moore for the valuable discussions on teams of autonomous mobile agents, T. Weiss for proofreading this paper, M. Morehead and S. Kemler for their help with the measurements, and the reviewers for carefully reading this paper and providing useful suggestions for its improvement.

References

[1] C. H. Mar and W. K. Seah, "An analysis of connectivity in a MANET of autonomous cooperative mobile agents under the Rayleigh fading channel," in *Proc. IEEE Veh. Technol. Conf.*, 2005, vol. 4, pp. 2606–2610.

[2] P. Basu and J. Redi, "Movement-control algorithms for realization of fault-tolerant ad hoc robot networks," *IEEE Netw.*, vol. 18, no. 4, pp. 36–44, Jul./Aug. 2004.

[3] I. Rubin and R. Zhang, "Performance behavior of unmanned vehicle aided mobile backbone based wireless ad hoc networks," in *Proc. IEEE Veh. Technol. Conf.*, 2003, vol. 2, pp. 955–959.

[4] C. Oestges, S. R. Saunders, and D. Vanhoenacker-Janvier, "Physical statistical modelling of the land mobile satellite channel based on ray tracing," *Proc. Inst. Electr. Eng.—Microwaves, Antennas Propagation*, vol. 146, no. 1, pp. 45–49, Feb. 1999.

[5] S. R. Saunders and B. G. Evans, "A physical model of shadowing probability for land mobile satellite propagation," *Electron. Lett.*, vol. 32, no. 17, pp. 1548–1549, Aug. 1996.

[6] E. Lutz, "The land and mobile satellite communication channel-recording statistics and channel model," *IEEE Trans. Veh. Technol.*, vol. 40, no. 2, pp. 375–386, May 1991.

[7] A. G. Emslie, R. L. Lagace, and P. F. Strong, "Theory of the propagation of UHF radio waves in coal mine tunnels," *IEEE Trans. Antennas Propag.*, vol. AP-23, no. 2, pp. 192–205, Mar. 1975.

[8] C. L. Holloway, D. A. Hill, R. A. Dalke, and G. A. Hufford, "Radio wave propagation characteristics in lossy circular waveguides such as tunnels, mine shafts, and boreholes," *IEEE Trans. Antennas Propag.*, vol. 48, no. 9, pp. 1354–1366, Sep. 2000.

[9] Y. Zhang, "Novel model for propagation loss prediction in tunnels," *IEEE Trans. Veh. Technol.*, vol. 52, no. 5, pp. 1308–1314, Sep. 2003.

[10] D. G. Dudley and H.-Y. Pao, "System identification for wireless propagation channels in tunnels," *IEEE Trans. Antennas Propag.*, vol. 53, no. 8, pp. 2400–2405, Aug. 2005.

[11] D. G. Dudley, M. Lienard, S. F. Mahmoud, and P. Degauque, "Wireless propagation in tunnels," *IEEE Antennas Propag. Mag.*, vol. 49, no. 2, pp. 11–26, Apr. 2007.

[12] Y. P. Zhang and Y. Hwang, "Characterization of UHF radio propagation channels in tunnel environments for microcellular and personal communications," *IEEE Trans. Veh. Technol.*, vol. 47, no. 1, pp. 283–296, Feb. 1998.

[13] Y. P. Zhang, G. X. Zheng, and J. H. Sheng, "Radio propagation at 900 MHz in underground coal mines," *IEEE Trans. Antennas Propag.*, vol. 49, no. 5, pp. 757–762, May 2001.

[14] H. R. Anderson, "Building corner diffraction measurements and predictions using UTD," *IEEE Trans. Antennas Propag.*, vol. 46, no. 2, pp. 292–293, Feb. 1998.

[15] Y. P. Zhang, Y. Hwang, and R. G. Kouyoumjian, "Ray-optical prediction of radio-wave propagation characteristics in tunnel environments—Part 2: Analysis and measurements," *IEEE Trans. Antennas Propag.*, vol. 46, no. 9, pp. 1337–1345, Sep. 1998.

[16] J. Lee and H. L. Bertoni, "Coupling at cross, T, and L junctions in tunnels and urban street canyons," *IEEE Trans. Antennas Propag.*, vol. 51, no. 5, pp. 926–935, May 2003.

[17] Y. Zhang and Y. Hwang, "Characterization of UHF radio propagation channel in curved tunnels," in *Proc. 7th IEEE Int. Symp. Pers., Indoor, Mobile Radio Commun.*, Oct. 1996, vol. 3, pp. 798–802.

[18] S. B. M. Lienard and P. Degauque, "Theoretical and experimental approach of the propagation at 2.5 GHz and 10 GHz in straight and curved tunnels," in *Proc. IEEE Veh. Technol. Conf.*, Amsterdam, The Netherlands, Sep. 1999, pp. 2268–2271.

[19] M. Nilsson, J. Slettenmark, and C. Beckman, "Wave propagation in curved road tunnels," in *Proc. Antennas Propag. Soc. Int. Symp.*, Jun. 1998, vol. 4, pp. 1876–1879.

[20] D. Didascalou, M. Döttling, T. Zwick, and W. Wiesbeck, "A novel ray-optical approach to model wave propagation in curved tunnels," in *Proc. IEEE Veh. Technol. Conf.*, Amsterdam, The Netherlands, Sep. 1999, pp. 2313–2317.
[21] M. Ndoh, G. Y. Delisle, and R. Le, "An approach to propagation prediction in a complex mine environment," in *Proc. 17th Int. Conf. Appl. Electromagn. Commun.*, Dubrovnik, Croatia, Oct. 2003, pp. 237–240.
[22] M. Boutin, S. Affes, C. Despins, and T. Denidni, "Statistical modelling of a radio propagation channel in an underground mine at 2.4 and 5.8 GHz," in *Proc. 61st IEEE Veh. Technol. Conf.*, Jun. 2005, vol. 1, pp. 78–81.
[23] C. Nerguizian, C. L. Despins, S. Affès, and M. Djadel, "Radio-channel characterization of an underground mine at 2.4 GHz," *IEEE Trans. Wireless Commun.*, vol. 4, no. 5, pp. 2441–2453, Sep. 2005.
[24] P. Shankar, *Introduction to Wireless Systems*. New York: Wiley, 2002.
[25] P. L. Meyer, *Introductory Probability and Statistical Applications*, 2nd ed. Reading, MA: Addison-Wesley, 1970.
[26] V. Erceg, L. J. Greenstein, S. Y. Tjandra, S. R. Parkoff, A. Gupta, B. Kulic, A. A. Julius, and R. Bianchi, "An empirically based path loss model for wireless channels in suburban environments," *IEEE J. Sel. Areas Commun.*, vol. 17, no. 7, pp. 1205–1211, Jul. 1999.

Manoja D. Weiss (S'97–M'01) received the B.S.E.E. degree from Grove City College, Grove City, PA, in 1993, the M.S.E.E. degree from Pennsylvania State University, University Park Campus, in 1995, and the Ph.D. degree from the University of Colorado, Boulder, in 2001. Her doctoral research was on high-efficiency microwave power amplifiers and their linearization.

From 2001 to 2003, she was a Microwave Engineer with Phiar Corporation, Boulder, where she designed and built nanometer-scale antennas at terahertz frequencies. Since 2003, she has been with the Colorado School of Mines, Golden, as an Assistant Professor with the Division of Engineering, within the Electrical Specialty. Her current research interests include wireless sensor networks, mobile ad hoc networks, and electromagnetic propagation in underground environments.

James Peak received the B.S.M.E. degree from the University of Colorado, Boulder, in 2003 and the M.S.E.S. (M.E.) degree from the Colorado School of Mines, Golden, in 2006.

He is currently with Lockheed Martin Space Systems Company Communications, Denver, CO. His research interests include control systems and autonomous mobile agents.

Thomas Schwengler (SM'07) received the Diplome d'Ingenieur degree from the Ecole Superieure d'Electricite, Gif Sur Yvette, France, and the M.S.E.E. and Ph.D. degrees in electrical engineering from the University of Colorado, Boulder.

He has been a Research Engineer with France Telecom R&D and the Director of RF Engineering with Qwest Wireless. He is currently with Qwest Communications, Denver, CO, and is an Adjunct Faculty Member of the University of Colorado Interdisciplinary Telecommunications Program. His research interests are RF engineering applied to wireless broadband communications, including propagation modeling and measurements, focusing on Wi-Fi and WiMAX systems.